SCIENTIFIC REP⚙RTS

OPEN

Extracting the Energy Sensitivity of Charge Carrier Transport and Scattering

Shuang Tang

It is a challenge to extract the energy sensitivity of charge carriers' transport and scattering from experimental data, although a theoretical estimation in which the existing scattering mechanism(s) are preliminarily assumed can be easily done. To tackle this problem, we have developed a method to experimentally determine the energy sensitivities, which can then serve as an important statistical measurement to further understand the collective behaviors of multi-carrier transport systems. This method is validated using a graphene system at different temperatures. Further, we demonstrate the application of this method to other two-dimensional (2D) materials as a guide for future experimental work on the optimization of materials performance for electronic components, Peltier coolers, thermoelectricity generators, thermocouples, thermopiles, electrical converters and other conductivity and/or Seebeck-effect-related sensors.

The study of charge carrier transport focuses on the collective behaviors of electrons and holes in both real space and momentum space under external force fields, especially electrical fields. Quantum transport can be observed in single-electron devices[1–6] and in highly ordered mesoscopic systems at cryogenic temperatures[7–13], but the statistical transport behavior of multiple carriers for most material systems in modern applications must be described by diffusive models, such as the Boltzmann equations[14–27].

Various scattering mechanisms may exist in diffusive transport[10,28–37]. Generally, the scattering strength and transport strength are inversely proportional to each other. By using an electrical conductivity (σ) matching method[10,33,38–48] or observations of fast laser-assisted photon-electron interactions[49–54], the average scattering time of carriers can be obtained and used to estimate the scattering strength. However, scattering and transport are also sensitive to the carrier energy. Therefore, if we can develop a method to extract the energy sensitivities of both carrier scattering and transport from experiments with real materials, we will have more instructive information on how to improve diffusive-transport-related applications in electronics, mechatronics and thermoelectronics.

The advancement of novel layered two-dimensional (2D) materials, including graphene[41,42,55–65], transition metal dichalcogenide (TMD) layers[66], and black phosphorene (BP)[67–71], has provided a convenient testing platform for developing an energy sensitivity extraction method. These materials have simple band structures, where only a single valley or a few degenerate valleys are involved in transport[72–81]. Further, the Fermi levels and carrier concentrations of these materials can be efficiently tuned[67,70,82–96]. The transport behavior of graphene carriers has been intensively studied[10,33,38–48,97] and can serve as a reliable system for testing new methods. Most importantly, this new method could also be used to improve the fundamental understanding of TMD and BP layers.

In this paper, we first define the energy sensitivities of carrier scattering and carrier transport within the diffusive transport regime. We then develop a new method to detect such energy sensitivities and test it in a graphene system at different temperatures. After that, we show how to use this method in other novel 2D material systems. Doing so will open a wide range of potential applications in transport-related research. For example, the method can provide information that can be used to analyze the major scattering sources in materials for conductivity improvement, to help engineer the types and concentrations of scattering centers to enhance the efficiency of Peltier cooling and/or thermoelectricity generating, and to help design various sensors, including thermocouples[98], thermopiles[98], electrical converters[99,100], vacuum sensors[101,102], flow sensors[103,104], radiation sensors[105,106], and special chemical sensors[107,108], using the Seebeck effect.

College of Engineering, State University of New York, Polytechnic Institute, Albany, New York, 12203, USA. Correspondence and requests for materials should be addressed to S.T. (email: tangs1@sunyit.edu)

Method

Within the diffusive transport regime, the relation between the carrier scattering and the transport, including the electrical conductivity (σ) and the Seebeck coefficient (S)[35,109], can be described by the Boltzmann equations. Rigorous solutions that include the elastic and inelastic scatterings in both degenerate and non-degenerate cases can be obtained by iterative approaches, e.g., Rode's method[36,110–118] (See the supplementary materials for further explanations). It is well known that under the relaxation time approximation, the transport properties can generally be approximated as

$$\sigma = q^2 \int \left(-\frac{\partial f_0}{\partial \varepsilon} \right) \Xi(\varepsilon) d\varepsilon \tag{1}$$

$$S = \frac{k_B}{q} \frac{\int \left(-\frac{\partial f_0}{\partial \varepsilon} \right) \Xi(\varepsilon)(\varepsilon - \varepsilon_f) d\varepsilon}{\int \left(-\frac{\partial f_0}{\partial \varepsilon} \right) \Xi(\varepsilon) d\varepsilon} \tag{2}$$

$$\Xi(\varepsilon) = \tau(\varepsilon) D(\varepsilon) \langle v^2 \rangle_\varepsilon \tag{3}$$

where q is the charge per carrier, T is the absolute temperature, k_B is the Boltzmann constant, ε is the reduced carrier energy (i.e., $\varepsilon = E/k_B T$), ε_f is the reduced Fermi level, f_0 is the Fermi-Dirac distribution, and $\Xi(\varepsilon)$, $\tau(\varepsilon)$, and $D(\varepsilon)$ are the transport distribution, scattering time and electronic density of states as a function of ε[31], respectively. Further, v is the group velocity of the carriers, and the operator $\langle \cdot \rangle_\varepsilon$ stands for the mean value on the constant energy surface. Here, $\langle v^2 \rangle_\varepsilon \propto \varepsilon^r$ and $r = 0$ ($r = 1$) for a linear (parabolic) band. $D(\varepsilon) \propto \varepsilon^l$ and $l = 1$ ($l = 0$) for a 2D linear (parabolic) band.

We can see that the transport properties are ultimately determined by the transport distribution $\Xi(\varepsilon)$. Without loss of generality, the strength of transport at an arbitrary energy $\varepsilon = \varepsilon_0$ can be characterized by $\theta = \Xi(\varepsilon_0)$. The energy sensitivity of transport can then be characterized by

$$s|_{\varepsilon_0} = \frac{d\Xi/\Xi}{d\varepsilon/\varepsilon} \bigg|_{\varepsilon_0}. \tag{4}$$

Generally, the energy sensitivity s is a function of the carrier energy, temperature and carrier valley. For a single carrier, it is a specific value, but for the collective behavior of multiple carriers, it is a statistical measurement of the whole system. These statistical measurements are commonly used for diffusive transport; e.g., the carrier mobility is a statistical measurement of how mobile the carriers behave under an electrical field. Similarly, the strength of scattering at an arbitrary $\varepsilon = \varepsilon_0$ can be characterized by $\xi = 1/\tau(\varepsilon_0)$, and the energy sensitivity of scattering can be characterized by

$$j|_{\varepsilon_0} = -\frac{d\zeta/\zeta}{d\varepsilon/\varepsilon} \bigg|_{\varepsilon_0}. \tag{5}$$

These two energy sensitivities (s and j) can be connected by Equation (3), e.g., $s = j + 1$, for a specific 2D band valley.

Intuitively, it is reasonable to expect that the same crowds of point defects will have weaker scattering effects (and, hence, stronger transport) to the higher energy carriers near a specific carrier pocket. The carrier energy sensitivity defined here can be then used to quantitatively evaluate the percent change in scattering/transport with respect to the percent change in carrier energy. This is unlike a traditional TEP model, where a presumed constant is used to simplify the model and calculations. Because TEP is not sensitive to transport data, the fit can generally be accepted; therefore, it does not provide a perspective on how the carriers' scattering and transport in different systems react to changes in the carrier energy. As we will prove below, the concept of carrier energy sensitivity is not a presumed constant but a physical quantity that can vary with the carriers, systems and scattering mechanisms. It is also sensitive to the maximum Seebeck coefficient and can therefore be detected with a relatively high accuracy and used to infer the scattering mechanisms.

The rigorous Seebeck coefficients can be calculated through iterative approaches, e.g., Rode's method[36,110–118]. Therefore, both elastic and inelastic scattering can be considered based on Equations (S14) and (S15).

Through our theoretical derivations, we have found that for a given band structure, the Seebeck coefficients for a specific Fermi level (i.e., carrier concentration) increase monotonically with the energy sensitivity of transport (s). Further, we have discovered that the maximum values of the Seebeck coefficients (S_m) form a near-linear relation with the energy sensitivity, i.e.,

$$S_m \approx s \frac{0.94 \, k_B}{q} + S_0, \tag{6}$$

where S_0 is a band-structure-specified quantity. A software application to observe this relation in a general case is written using Matlab for this paper. These findings imply that once we have measured the S_m values of a system at a specific temperature, we can deduce the energy sensitivity of transport s (and, thus, the energy sensitivity of scattering j) at this temperature. Generally, there will be only one local optimal Seebeck coefficient corresponding to
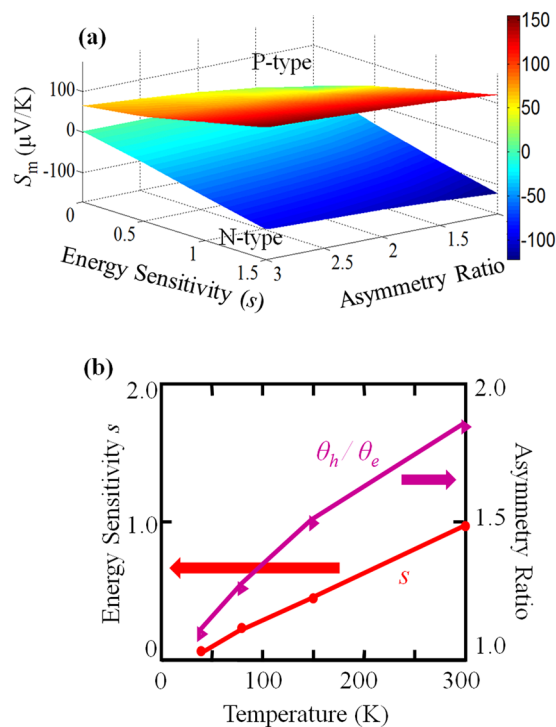
Figure 1. The new method was validated using a graphene system. (**a**) Plots of the optimal Seebeck coefficient (S_m) of graphene are presented for both N-type and P-type regimes, as a function of energy sensitivity (s) and the asymmetry ratio of scattering strength θ_h/θ_e at 300 K. (**b**) The results of the energy sensitivity (s) and asymmetry ratio (θ_h/θ_e) of carrier scatterings near the band valley in graphene correspond to the data in Table 1.

Temperature (K)	300	150	80	40
P-type S_m (μV/K)	92.52	57.94	33.64	14.95
N-type S_m (μV/K)	−59.81	−39.25	−24.30	−10.28

Table 1. Measured Optimal Seebeck Coefficient[84] for the Graphene on a SiO_2 substrate[84].

each band valley. Therefore, for a materials system with single- or degenerate-valley transport, such as 2D layered materials, the valley-specific energy sensitivity can be deduced directly. For a material with non-degenerate-valley transport, multiple local optimums of the Seebeck coefficient should be considered for the deduction. Once the energy sensitivity of transport (s) is measured with this method, the energy sensitivity of scattering (j) can be naturally obtained. For a material with a single scattering channel, j is simply the channel-specific energy sensitivity. For a case with multiple scattering channels, j is the effective energy sensitivity that represents a weighted average of all existing channels, which is also a statistical measurement.

Method Validation

Now, we test this method in a graphene system. With the development of nanotechnology for device fabrication, the measurement of Seebeck coefficient (S) as a function of Fermi level is now available[82–91]. The carriers that contribute to electronic transport come mainly from the two isotropic Dirac cones, whose apexes are near the Fermi level in the first Brillouin zone. The rigorous Seebeck coefficient can be calculated using the iterative approaches method[36,110–118]. Therefore, both the elastic and inelastic scatterings can be considered based on Equations (S14) and (S15). For convenience of calculation, we can first calculate a map of S_m as a function of s and $\gamma = \theta_h/\theta_e$ for both the P- and N-type regimes. This S_m map will vary with temperature. We illustrated an example at $T = 300$ K in Fig. 1(a). Then, by matching the measured values of S_m to this map, we can obtain a single solution set for s and $\gamma = \theta_h/\theta_e$ at each temperature. The S_m values of graphene at different temperatures have been measured in previous reports[82–91]. Using ref.[84] as an example, where a graphene system on a SiO_2 substrate is measured using a gated thermoelectric device with Fermi level tuning. The configuration used for the experimental setup is explained in Fig. 1 of ref.[84]. Their data are summarized in Table 1. We then determined the values of the energy sensitivity of transport s and the asymmetry ratio $\gamma = \theta_h/\theta_e$ at each temperature, according to Table 1. Our results are shown in Fig. 1(b).

From Fig. 1(b), we see that the energy sensitivity s changes significantly with temperature, which implies that the effective carrier scattering mechanism is very temperature-sensitive. When approaching the low temperature end, the energy-sensitivity behaves as $s \to 0$, which implies that $\tau^{-1} \to \tau^{-1} \propto D(\varepsilon)$, and the scattering is negatively sensitive to the energy of carriers. When approaching high temperatures end, the sensitivity behaves as
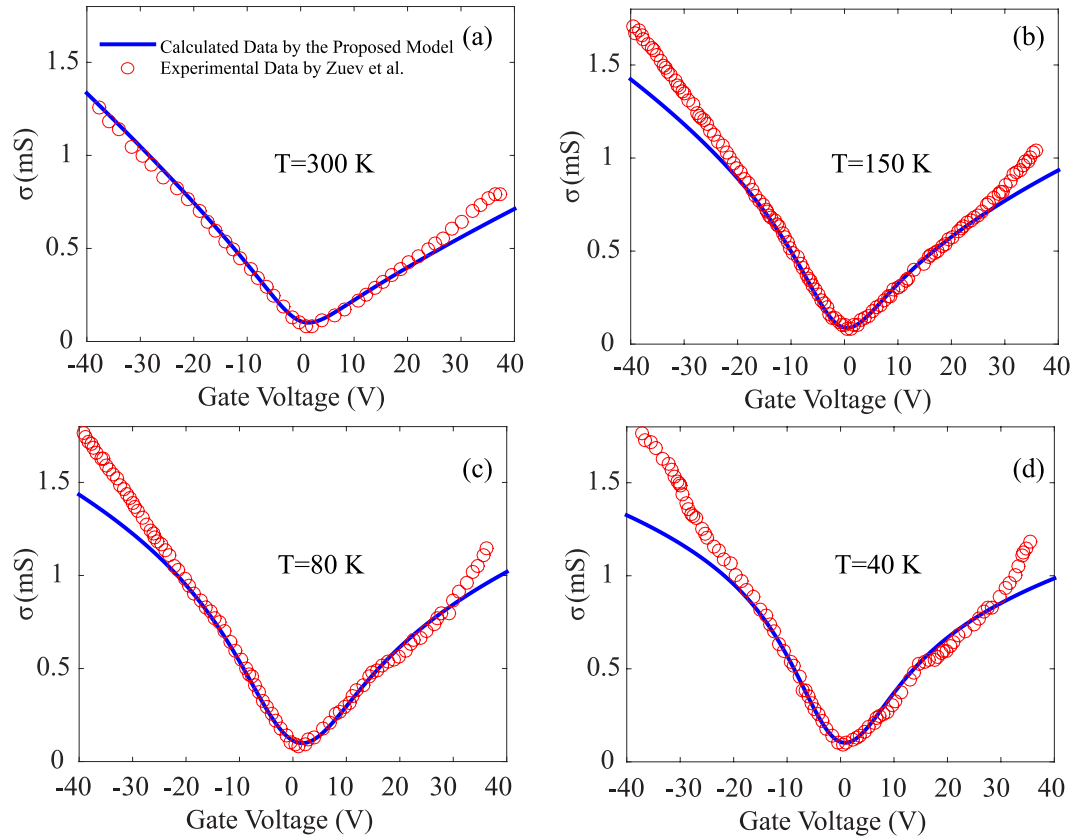
Figure 2. Comparison between the electrical conductivity (σ) data at (**a**) 300 K, (**b**) 150 K, (**c**) 80 K and (**d**) 40 K, as determined by the proposed model (blue lines) and experimental measurement (red circles)[84]. It can be seen that the model is generally quite consistent with the experimental data.

$s \to 1$, which implies that τ tends to become constant over a different range of carrier energies. This information about $\tau(\varepsilon)$ can be explained by the scattering mechanism(s) of graphene carriers. In the low temperature range, the dominant scattering mechanisms should be acoustic phonon scattering and short-range disorder scattering, such as surface roughness[119–121], point defects and vacancies[122], that are intrinsically formed by the carbon atoms within the graphene sheet. For these scattering mechanisms, the scattering time $\tau(\varepsilon)$ will be inversely proportional to the density of states $D(\varepsilon)$[120,123]. Equation (3) then suggests that $s \to 0$. The small deviation of s from 0 might be due to minor scattering mechanism(s) or may occur because the dispersion relation can be disturbed from linearity to a certain extent near the apex of Dirac cones[124–126]. At elevated temperatures, the inelastic scattering due to the optical phonons becomes important. The scattering time for such inelastic scattering is usually constant over a range of carrier energies, i.e., $j = 0$, either by the rigorous solution or the relaxation time approximation of the Boltzmann equation, which is consistent with the results. On the other hand, at elevated temperatures, the carrier scattering mechanism(s) induce higher values of j, which then become(s) important; e.g., thermal ripple scattering[119,127–130] will have $j = 2$. This high-j scattering now coexists with and compensates for the low-j scatterings, e.g., the acoustic phonon scattering ($j = -1$), which makes the statistical $j \to 0$, i.e., $s \to 1$.

Another important trend is shown in Fig. 1(b), where the asymmetry ratio θ_h/θ_e increases with temperature, but the electrons and the holes are close to being symmetric at temperatures as low as 40 K. This is consistent with the previous report that electrons and holes are asymmetric when they transported in graphene-related systems[131], even though they are symmetric in the dispersion relation. Furthermore, the scattering strengths for electrons and holes deduced from this new approach are $\xi_e = 0.5 \times 10^{14} \text{s}^{-1}$ and $\xi_h = 2.63 \times 10^{13} \text{s}^{-1}$ at 300 K, respectively. Further, in our above calculations for graphene, we assume that the electronic transport comes from only the carriers near the apex of the Dirac cones, and ignoring the contributions from higher energy carriers. To evaluate how this deviates from reality, we compared the electrical conductivity data from the above model to experimental measurements at different temperatures, as shown in Fig. 2. Although we are now considering only the two band valleys of the Dirac cone, the modeled data are already quite consistent with the experimental measurements. The deviations at higher energy occur because more bands are contributing to the transport.

Traditionally, Mott's relation is used to model the Seebeck coefficient, where

$$S_{Mott}(E_f) = -\frac{\pi^2}{3qk_B\sigma}\left(\frac{\partial\sigma}{\partial\varepsilon}\right)_{\varepsilon_f},$$
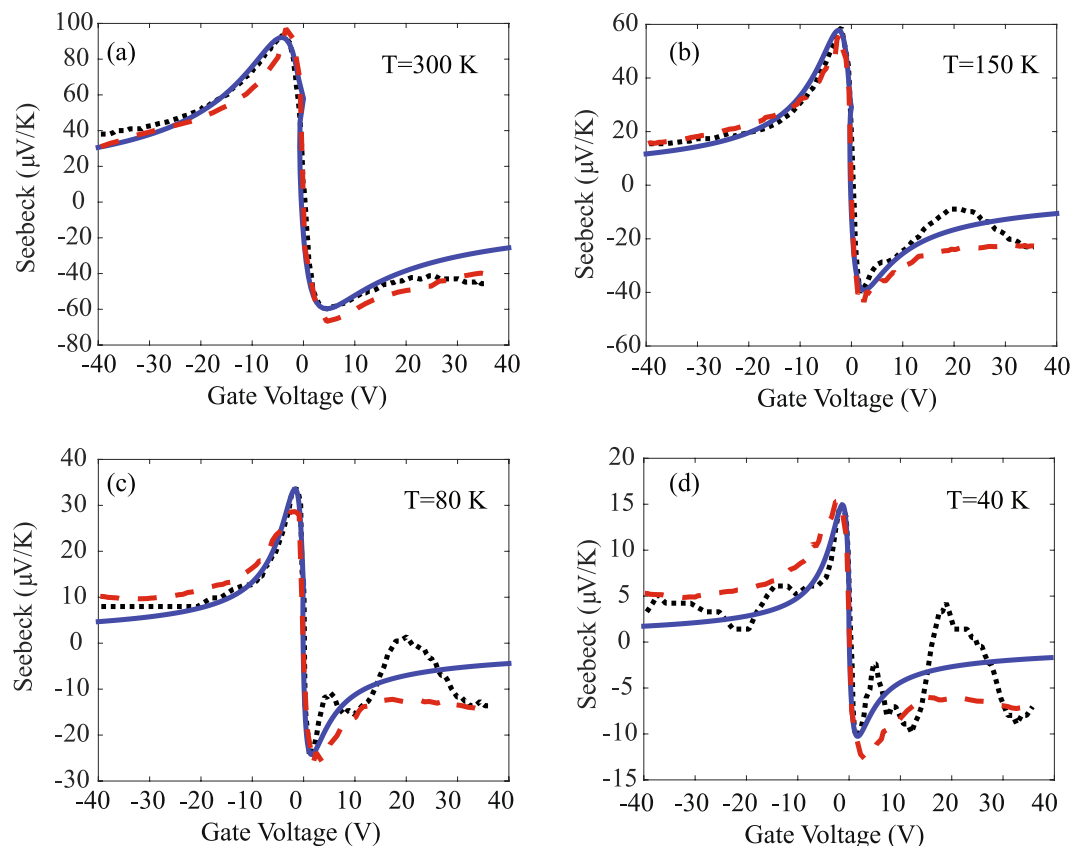
(7)

Figure 3. Comparison of the Seebeck coefficient data from experimental measurements (dotted lines), the Mott's relation (dashed lines) and the proposed model (solid lines). It can be seen that the proposed model is generally more accurate than Mott's relation for data near the Seebeck peak, especially at lower temperatures.

which suggests that the Seebeck coefficient can be simply obtained from the electrical conductivity data. However, our theoretical derivation has noted that the Mott's relation is only suitable to obtain Seebeck coefficients that are far from the optimal points. To further demonstrate this, we have compared the Seebeck coefficient values from the experiments, the Mott's relation, and our proposed model, as shown in Fig. 3. In the graphene system, the proposed method is generally better than Mott's relation for Seebeck data near the peak, and the advantage of the proposed method becomes increasingly obvious at lower temperatures.

Discussion

Now, we use the new method to study other layered 2D materials. TMD monolayers are another class of 2D materials[73–81], where the transport involved band valleys at the *K* and *K'* points are degenerate for the conduction side and valence side. The electrons and holes are parabolically dispersed at the band edges. Figure 4(a) shows the results for how the energy sensitivity of transport is derived from the optimal values of the Seebeck coefficient with our new method. The one-to-one correspondence and linear relation still hold for various TMD monolayer systems. BP is another novel layered 2D material with parabolically dispersed band edges located at the *Γ* point in the Brillouin zone[70,132–135]. Figure 4(b) shows how the energy sensitivity of transport can be solved from the optimal values of the Seebeck coefficient for a single layer of BP. Both the Γ-X and Γ-Y directions are exhibited for anisotropic transport in BP[136–138]. Details on modeling an anisotropic system are given in the supplementary materials and in ref.[109].

Most of these novel layered 2D materials have single-valley scattering and are therefore an ideal starting point for this new method. For a band structure that involves multiple non-degenerate band valleys in transport, each valley will induce a peak or kink in the Seebeck coefficient vs. Fermi level curve. Therefore, to extend the new method to such a general system, the non-primary peaks or kinks of the Seebeck coefficient will be used to solve the values of energy sensitivity (*s*).

Further, we know that for ballistic transport[139–142],

$$\sigma = q^2 \int \left(-\frac{\partial f_0}{\partial \varepsilon} \right) \mathbf{T}(\varepsilon) d\varepsilon \tag{8}$$
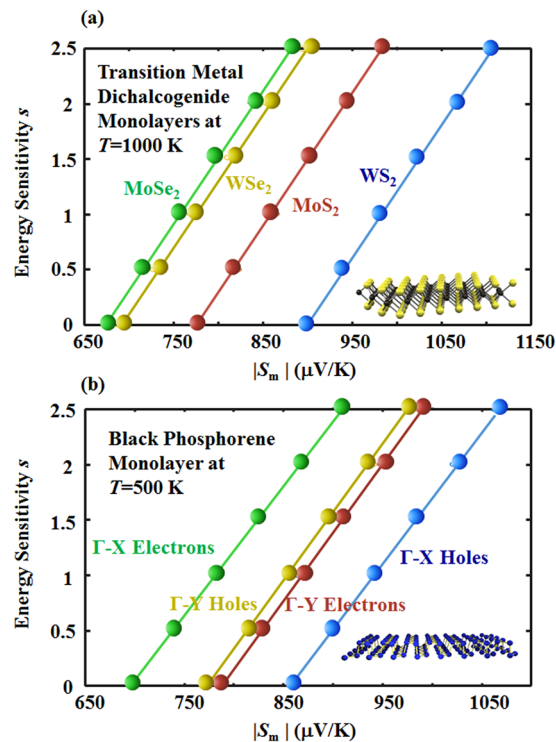
Figure 4. How the optimal Seebeck coefficient (S_m) can be used to infer the energy sensitivity of transport (s) for various (**a**) TMD monolayers and (**b**) black phosphorene monolayer. The filled dots show calculated data, and the solid curves show a fitted linear relation from these data for each type of 2D materials system. The band valleys of the electrons and holes in black phosphorene are anisotropic, and both the Γ-X and Γ-Y directions are illustrated here. The general approach for modeling an anisotropic system is discussed in the supplementary materials, and details can be found in ref.[109].

$$S = \frac{k_B}{q} \frac{\int \left(-\frac{\partial f_0}{\partial \varepsilon} \right) \mathbf{T}(\varepsilon)(\varepsilon - \varepsilon_f) d\varepsilon}{\int \left(-\frac{\partial f_0}{\partial \varepsilon} \right) \mathbf{T}(\varepsilon) d\varepsilon}$$

(9)

where $\mathbf{T}$ is the total transmission probability function. Equations (1) and (2) are exactly the same as Equations (8) and (9), except for the definitions of Ξ and $\mathbf{T}$. Therefore, we can use Ξ as a broader function: Ξ serves as the transport distribution function for diffusive channels and the total transmission probability for ballistic channels, and it can describe the combination of multiple mixed channels. Therefore, the energy sensitivity can be measured using this more general function, Ξ.

Conclusion

Based on our theoretical derivations and numerical validations, we have proposed that the optimum values of the Seebeck coefficient can be used as a new tool to extract the carrier energy sensitivity of transport and scattering from experimental data. This statistical measurement can provide us with deeper information to improve applications related to diffusive transfer in semiconducting and metallic materials. We have validated this new method using a graphene system at different temperatures. Then, we have shown how to use the validated method for other layered 2D materials, including various transition metal dichalcogenide layers and a black phosphorene layer. This will allow a wide range of potential applications in transport-related research, including electronic devices, Peltier coolers, thermoelectricity generators, thermocouples, thermopiles, electrical converters, and other sensors using the Seebeck effect, e.g., vacuum sensors, flow sensors, radiation sensors, and chemical sensors.

References

1. Ubbelohde, N., Fricke, C., Flindt, C., Hohls, F. & Haug, R. J. Measurement of finite-frequency current statistics in a single-electron transistor. *Nature communications* **3**, 612 (2012).
2. Lee, S., Lee, Y., Song, E. B. & Hiramoto, T. Observation of single electron transport via multiple quantum states of a silicon quantum dot at room temperature. *Nano letters* **14**, 71–77 (2013).
3. Tyszka, K. *et al*. Comparative study of donor-induced quantum dots in Si nano-channels by single-electron transport characterization and Kelvin probe force microscopy. *Journal of Applied Physics* **117**, 244307 (2015).
4. Küng, B. *et al*. Test of the fluctuation theorem for single-electron transport. *Journal of Applied Physics* **113**, 136507 (2013).
5. Caillard, L. *et al*. Gold nanoparticles on oxide-free silicon–molecule interface for single electron transport. *Langmuir* **29**, 5066–5073 (2013).

6. Jezouin, S. *et al*. Quantum limit of heat flow across a single electronic channel. *Science* **342**, 601–604 (2013).
7. Kolkowitz, S. *et al*. Probing Johnson noise and ballistic transport in normal metals with a single-spin qubit. *Science* **347**, 1129–1132 (2015).
8. Prosen, T. Open X X Z Spin Chain: Nonequilibrium Steady State and a Strict Bound on Ballistic Transport. *Physical review letters* **106**, 217206 (2011).
9. Bermúdez, A., Bruderer, M. & Plenio, M. Controlling and measuring quantum transport of heat in trapped-ion crystals. *Physical review letters* **111**, 040601 (2013).
10. Sarma, S. D., Adam, S., Hwang, E. & Rossi, E. Electronic transport in two-dimensional graphene. *Reviews of Modern Physics* **83**, 407 (2011).
11. Bao, W. *et al*. Stacking-dependent band gap and quantum transport in trilayer graphene. *Nature Physics* **7**, 948 (2011).
12. Trescher, M., Sbierski, B., Brouwer, P. W. & Bergholtz, E. J. Quantum transport in Dirac materials: signatures of tilted and anisotropic Dirac and Weyl cones. *Physical Review B* **91**, 115135 (2015).
13. Tayran, C. *et al*. Optimizing Electronic Structure and Quantum Transport at the Graphene-Si (111) Interface: An Ab Initio Density-Functional Study. *Physical review letters* **110**, 176805 (2013).
14. Bilc, D. I., Hautier, G., Waroquiers, D., Rignanese, G.-M. & Ghosez, P. Low-dimensional transport and large thermoelectric power factors in bulk semiconductors by band engineering of highly directional electronic states. *Physical review letters* **114**, 136601 (2015).
15. Hinsche, N. F. *et al*. Impact of the topological surface state on the thermoelectric transport in Sb2Te3 thin films. *Acs Nano* **9**, 4406–4411 (2015).
16. Zhou, J., Yang, R., Chen, G. & Dresselhaus, M. S. Optimal bandwidth for high efficiency thermoelectrics. *Physical review letters* **107**, 226601 (2011).
17. Li, S., Jia, X. & Ma, H. First-principles investigation of electronic structure and transport properties of CoSb3 under different pressures. *Chemical Physics Letters* **549**, 22–26 (2012).
18. Chang, P.-H., Bahramy, M. S., Nagaosa, N. & Nikolic, B. K. Giant thermoelectric effect in graphene-based topological insulators with heavy adatoms and nanopores. *Nano letters* **14**, 3779–3784 (2014).
19. Azam, S. & Reshak, A. Transport properties of APdCu (Se 2)(Se 3)(A = K and Rb): new quaternary copper palladium polyselenides. *RSC Advances* **4**, 20102–20113 (2014).
20. Pal, K., Anand, S. & Waghmare, U. V. Thermoelectric properties of materials with nontrivial electronic topology. *Journal of Materials Chemistry C* **3**, 12130–12139 (2015).
21. Neophytou, N. & Kosina, H. Bias-induced hole mobility increase in narrow [111] and [110] Si nanowire transistors. *IEEE Electron Device Letters* **33**, 652–654 (2012).
22. Gluschke, J. G. *et al*. Characterization of Ambipolar GaSb/InAs Core–Shell Nanowires by Thermovoltage Measurements. *Acs Nano* **9**, 7033–7040 (2015).
23. Lee, J.-H. Significant enhancement in the thermoelectric performance of strained nanoporous Si. *Physical Chemistry Chemical Physics* **16**, 2425–2429 (2014).
24. Zhou, G. & Wang, D. Few-quintuple Bi 2 Te 3 nanofilms as potential thermoelectric materials. *Scientific reports* **5**, 8099 (2015).
25. Wierzbowska, M., Dominiak, A. & Pizzi, G. Effect of C-face 4H-SiC (0001) deposition on thermopower of single and multilayer graphene in AA, AB and ABC stacking. *2D Materials* **1**, 035002 (2014).
26. Van Quang, T. & Kim, M. Effect on the Electronic, Magnetic and Thermoelectric Properties of Bi_2Te_3 by the Cerium Substitution. *IEEE Transactions on Magnetics* **50**, 1–4 (2014).
27. Parker, D., Chen, X. & Singh, D. J. High three-dimensional thermoelectric performance from low-dimensional bands. *Physical review letters* **110**, 146601 (2013).
28. Chasmar, R. & Stratton, R. The thermoelectric figure of merit and its relation to thermoelectric generators. *International journal of electronics* **7**, 52–72 (1959).
29. Vining, C. B. A model for the high-temperature transport properties of heavily doped n-type silicon-germanium alloys. *Journal of Applied Physics* **69**, 331–341 (1991).
30. Singh, J. *Physics of Semiconductors and their Heterostructures*. (McGraw-Hill College, 1993).
31. Sofo, J. & Mahan, G. Optimum band gap of a thermoelectric material. *Physical Review B* **49**, 4565 (1994).
32. Ohta, S., Nomura, T., Ohta, H. & Koumoto, K. High-temperature carrier transport and thermoelectric properties of heavily La-or Nb-doped Sr Ti O 3 single crystals. *Journal of Applied Physics* **97**, 034106 (2005).
33. Stauber, T., Peres, N. & Guinea, F. Electronic transport in graphene: A semiclassical approach including midgap states. *Physical Review B* **76**, 205423 (2007).
34. Teramoto, T. *et al*. Influence of the band structure of BiSb alloy on the magneto-Seebeck coefficient. *Journal of Applied Physics* **104**, 053714 (2008).
35. Goldsmid, H. J. *Introduction to thermoelectricity*. Vol. 121 (Springer, 2010).
36. Lundstrom, M. *Fundamentals of carrier transport*. (Cambridge university press, 2009).
37. Minnich, A. *et al*. Modeling study of thermoelectric SiGe nanocomposites. *Physical Review B* **80**, 155327 (2009).
38. Cheianov, V. V. & Fal'ko, V. I. Friedel oscillations, impurity scattering, and temperature dependence of resistivity in graphene. *Physical review letters* **97**, 226801 (2006).
39. Nomura, K. & MacDonald, A. H. Quantum Hall ferromagnetism in graphene. *Physical review letters* **96**, 256602 (2006).
40. Hwang, E., Adam, S. & Sarma, S. D. Carrier transport in two-dimensional graphene layers. *Physical review letters* **98**, 186806 (2007).
41. Tan, Y.-W. *et al*. Measurement of scattering rate and minimum conductivity in graphene. *Physical review letters* **99**, 246803 (2007).
42. Chen, J.-H. *et al*. Charged-impurity scattering in graphene. *Nature Physics* **4**, 377 (2008).
43. Chen, F., Xia, J. & Tao, N. Ionic screening of charged-impurity scattering in graphene. *Nano letters* **9**, 1621–1625 (2009).
44. Chen, J.-H., Jang, C., Xiao, S., Ishigami, M. & Fuhrer, M. S. Intrinsic and extrinsic performance limits of graphene devices on SiO 2. *Nature nanotechnology* **3**, 206 (2008).
45. Bolotin, K., Sikes, K., Hone, J., Stormer, H. & Kim, P. Temperature-dependent transport in suspended graphene. *Physical review letters* **101**, 096802 (2008).
46. Du, X., Skachko, I., Barker, A. & Andrei, E. Y. Approaching ballistic transport in suspended graphene. *Nature nanotechnology* **3**, 491 (2008).
47. Hwang, E. & Sarma, S. D. Acoustic phonon scattering limited carrier mobility in two-dimensional extrinsic graphene. *Physical Review B* **77**, 115449 (2008).
48. Katsnelson, M., Guinea, F. & Geim, A. Scattering of electrons in graphene by clusters of impurities. *Physical Review B* **79**, 195426 (2009).
49. Dawlaty, J. M., Shivaraman, S., Chandrashekhar, M., Rana, F. & Spencer, M. G. Measurement of ultrafast carrier dynamics in epitaxial graphene. *Applied Physics Letters* **92**, 042116 (2008).
50. George, P. A. *et al*. Ultrafast optical-pump terahertz-probe spectroscopy of the carrier relaxation and recombination dynamics in epitaxial graphene. *Nano letters* **8**, 4248–4251 (2008).
51. Sun, D. *et al*. Ultrafast relaxation of excited Dirac fermions in epitaxial graphene using optical differential transmission spectroscopy. *Physical review letters* **101**, 157402 (2008).

52. Lui, C. H., Mak, K. F., Shan, J. & Heinz, T. F. Ultrafast photoluminescence from graphene. *Physical review letters* **105**, 127404 (2010).
53. Winnerl, S. *et al.* Carrier relaxation in epitaxial graphene photoexcited near the Dirac point. *Physical review letters* **107**, 237401 (2011).
54. Gabor, N. M. *et al.* Hot carrier–assisted intrinsic photoresponse in graphene. *Science* **334**, 648–652 (2011).
55. Novoselov, K. S. *et al.* Electric field effect in atomically thin carbon films. *Science* **306**, 666–669 (2004).
56. Charlier, J.-C. & Issi, J.-P. Electronic structure and quantum transport in carbon nanotubes. *Applied Physics A: Materials Science & Processing* **67**, 79–87 (1998).
57. Katsnelson, M., Novoselov, K. & Geim, A. Chiral tunnelling and the Klein paradox in graphene. *Nature Physics* **2**, 620 (2006).
58. Aleiner, I. & Efetov, K. Effect of disorder on transport in graphene. *Physical review letters* **97**, 236801 (2006).
59. Altland, A. Low-energy theory of disordered graphene. *Physical review letters* **97**, 236802 (2006).
60. Tworzydło, J., Trauzettel, B., Titov, M., Rycerz, A. & Beenakker, C. W. Sub-Poissonian shot noise in graphene. *Physical review letters* **96**, 246802 (2006).
61. Huard, B. *et al.* Transport measurements across a tunable potential barrier in graphene. *Physical review letters* **98**, 236803 (2007).
62. Williams, J., DiCarlo, L. & Marcus, C. Quantum Hall effect in a gate-controlled pn junction of graphene. *Science* **317**, 638–641 (2007).
63. Özyilmaz, B. *et al.* Electronic transport and quantum hall effect in bipolar graphene p− n− p junctions. *Physical review letters* **99**, 166804 (2007).
64. Bardarson, J. H., Tworzydło, J., Brouwer, P. & Beenakker, C. One-parameter scaling at the Dirac point in graphene. *Physical review letters* **99**, 106801 (2007).
65. Dubois, S.-M., Zanolli, Z., Declerck, X. & Charlier, J.-C. Electronic properties and quantum transport in Graphene-based nanostructures. *The European Physical Journal B* **72**, 1–24 (2009).
66. Ramakrishna Matte, H. *et al.* MoS2 and WS2 analogues of graphene. *Angewandte Chemie International Edition* **49**, 4059–4062 (2010).
67. Li, L. *et al.* Black phosphorus field-effect transistors. *Nature nanotechnology* **9**, 372 (2014).
68. Mehboudi, M. *et al.* Strain and the optoelectronic properties of nonplanar phosphorene monolayers. *Proceedings of the National Academy of Sciences* **112**, 5888–5892 (2015).
69. Fei, R. & Yang, L. Strain-engineering the anisotropic electrical conductance of few-layer black phosphorus. *Nano letters* **14**, 2884–2889 (2014).
70. Liu, H. *et al.* Phosphorene: an unexplored 2D semiconductor with a high hole mobility. *Acs Nano* **8**, 4033–4041 (2014).
71. Kim, J. *et al.* Observation of tunable band gap and anisotropic Dirac semimetal state in black phosphorus. *Science* **349**, 723–726 (2015).
72. Neto, A. C., Guinea, F., Peres, N. M., Novoselov, K. S. & Geim, A. K. The electronic properties of graphene. *Reviews of Modern Physics* **81**, 109 (2009).
73. Johari, P. & Shenoy, V. B. Tuning the electronic properties of semiconducting transition metal dichalcogenides by applying mechanical strains. *Acs Nano* **6**, 5449–5456 (2012).
74. Wang, Q. H., Kalantar-Zadeh, K., Kis, A., Coleman, J. N. & Strano, M. S. Electronics and optoelectronics of two-dimensional transition metal dichalcogenides. *Nature nanotechnology* **7**, 699 (2012).
75. Song, Y. & Dery, H. Transport theory of monolayer transition-metal dichalcogenides through symmetry. *Physical review letters* **111**, 026601 (2013).
76. Chhowalla, M. *et al.* The chemistry of two-dimensional layered transition metal dichalcogenide nanosheets. *Nature chemistry* **5**, 263 (2013).
77. Liu, G.-B., Shan, W.-Y., Yao, Y., Yao, W. & Xiao, D. Three-band tight-binding model for monolayers of group-VIB transition metal dichalcogenides. *Physical Review B* **88**, 085433 (2013).
78. Ghorbani-Asl, M., Borini, S., Kuc, A. & Heine, T. Strain-dependent modulation of conductivity in single-layer transition-metal dichalcogenides. *Physical Review B* **87**, 235434 (2013).
79. Kormányos, A., Zólyomi, V., Drummond, N. D. & Burkard, G. Spin-orbit coupling, quantum dots, and qubits in monolayer transition metal dichalcogenides. *Physical Review X* **4**, 011034 (2014).
80. Lv, R. *et al.* Transition metal dichalcogenides and beyond: synthesis, properties, and applications of single-and few-layer nanosheets. *Accounts of chemical research* **48**, 56–64 (2014).
81. Jariwala, D., Sangwan, V. K., Lauhon, L. J., Marks, T. J. & Hersam, M. C. Emerging device applications for semiconducting two-dimensional transition metal dichalcogenides. *Acs Nano* **8**, 1102–1120 (2014).
82. Kinany-Alaoui, M., Piraux, L., Issi, J., Pernot, P. & Vangelisti, R. Thermal conductivity and thermopower enhancement in magnetic acceptor graphite intercalation compounds. *Solid state communications* **68**, 1065–1068 (1988).
83. Piraux, L. *et al.* Transport properties in graphite intercalation compounds with transition metal fluorides. *Solid state communications* **82**, 371–375 (1992).
84. Zuev, Y. M., Chang, W. & Kim, P. Thermoelectric and magnetothermoelectric transport measurements of graphene. *Physical review letters* **102**, 096807 (2009).
85. Li, X., Yin, J., Zhou, J., Wang, Q. & Guo, W. Exceptional high Seebeck coefficient and gas-flow-induced voltage in multilayer graphene. *Applied Physics Letters* **100**, 183108 (2012).
86. Kim, G. H., Hwang, D. H. & Woo, S. I. Thermoelectric properties of nanocomposite thin films prepared with poly (3, 4-ethylenedioxythiophene) poly (styrenesulfonate) and graphene. *Physical Chemistry Chemical Physics* **14**, 3530–3536 (2012).
87. Basko, D. A photothermoelectric effect in graphene. *Science* **334**, 610–611 (2011).
88. Wang, D. & Shi, J. Effect of charged impurities on the thermoelectric power of graphene near the Dirac point. *Physical Review B* **83**, 113403 (2011).
89. Wang, L. *et al.* Large thermoelectric power factor in polyaniline/graphene nanocomposite films prepared by solution-assistant dispersing method. *Journal of Materials Chemistry A* **2**, 11107–11113 (2014).
90. Reshak, A., Khan, S. A. & Auluck, S. Thermoelectric properties of a single graphene sheet and its derivatives. *Journal of Materials Chemistry C* **2**, 2346–2352 (2014).
91. Lee, E.-S., Cho, S., Lyeo, H.-K. & Kim, Y.-H. Seebeck effect at the atomic scale. *Physical review letters* **112**, 136601 (2014).
92. Wu, J. *et al.* Large thermoelectricity via variable range hopping in chemical vapor deposition grown single-layer MoS2. *Nano letters* **14**, 2730–2734 (2014).
93. Dobusch, L. *et al.* Electric field modulation of thermovoltage in single-layer MoS2. *Applied Physics Letters* **105**, 253103 (2014).
94. Kim, J. S. *et al.* Dual gate black phosphorus field effect transistors on glass for NOR logic and organic light emitting diode switching. *Nano letters* **15**, 5778–5783 (2015).
95. Buscema, M. *et al.* Fast and broadband photoresponse of few-layer black phosphorus field-effect transistors. *Nano letters* **14**, 3347–3352 (2014).
96. Buscema, M., Groenendijk, D. J., Steele, G. A., Van Der Zant, H. S. & Castellanos-Gomez, A. Photovoltaic effect in few-layer black phosphorus PN junctions defined by local electrostatic gating. *Nature communications* **5**, 4651 (2014).
97. Young, A. *et al.* Tunable symmetry breaking and helical edge transport in a graphene quantum spin Hall state. *Nature* **505**, 528 (2014).
98. Van Herwaarden, A. & Sarro, P. Thermal sensors based on the Seebeck effect. *Sensors and Actuators* **10**, 321–346 (1986).

99. Baltes, H., Paul, O. & Brand, O. Micromachined thermally based CMOS microsensors. *Proceedings of the IEEE* **86**, 1660–1678 (1998).
100. Miyako, E. *et al.* A Photo-Thermal-Electrical Converter Based On Carbon Nanotubes for Bioelectronic Applications. *Angewandte Chemie International Edition* **50**, 12266–12270 (2011).
101. Fedder, G. K., Howe, R. T., Liu, T.-J. K. & Quevy, E. P. Technologies for cofabricating MEMS and electronics. *Proceedings of the IEEE* **96**, 306–322 (2008).
102. Elwenspoek, M. & Wiegerink, R. *Mechanical microsensors*. (Springer Science & Business Media, 2012).
103. Van Oudheusden, B. Silicon thermal flow sensors. *Sensors and Actuators A: Physical* **30**, 5–26 (1992).
104. Kirihara, A. *et al.* Flexible heat-flow sensing sheets based on the longitudinal spin Seebeck effect using one-dimensional spin-current conducting films. *Scientific reports* **6**, 23114 (2016).
105. Fraden, J. *Handbook of modern sensors: physics, designs, and applications*. (Springer Science & Business Media, 2004).
106. Wang, D.-b & Liao, X.-p A terminating-type MEMS microwave power sensor and its amplification system. *Journal of Micromechanics and Microengineering* **20**, 075021 (2010).
107. Tung, T. T. *et al.* Hybrid films of graphene and carbon nanotubes for high performance chemical and temperature sensing applications. *Small* **11**, 3485–3493 (2015).
108. Hierlemann, A., Brand, O., Hagleitner, C. & Baltes, H. Microfabrication techniques for chemical/biosensors. *Proceedings of the IEEE* **91**, 839–863 (2003).
109. Tang, S. & Dresselhaus, M. S. Anisotropic transport for parabolic, non-parabolic, and linear bands of different dimensions. *Applied Physics Letters* **105**, 033907 (2014).
110. Rode, D. Electron mobility in direct-gap polar semiconductors. *Physical Review B* **2**, 1012 (1970).
111. Willardson, R. K. & Beer, A. C. *Semiconductors and semimetals*. Vol. 12 (Academic press, 1977).
112. Miller, N. *et al.* Effect of charged dislocation scattering on electrical and electrothermal transport in n-type InN. *Physical Review B* **84**, 075315 (2011).
113. Ng, G., Vasileska, D. & Schroder, D. Calculation of the electron Hall mobility and Hall scattering factor in 6 H-SiC. *Journal of Applied Physics* **106**, 053719 (2009).
114. Ferry, D. *Semiconductor transport*. (CRC Press, 2000).
115. Ramu, A. T. *et al.* Rigorous calculation of the Seebeck coefficient and mobility of thermoelectric materials. *Journal of Applied Physics* **107**, 083707 (2010).
116. Ramu, A. T. *et al.* Thermoelectric transport in the coupled valence-band model. *Journal of Applied Physics* **109**, 033704 (2011).
117. Ramu, A. T. & Bowers, J. E. The impact of commonly used approximations on the computation of the Seebeck coefficient and mobility of polar semiconductors. *Applied Physics Letters* **101**, 173905 (2012).
118. Faghaninia, A., Ager, J. W. III & Lo, C. S. Ab initio electronic transport model with explicit solution to the linearized Boltzmann transport equation. *Physical Review B* **91**, 235123 (2015).
119. Katsnelson, M. & Geim, A. Electron scattering on microscopic corrugations in graphene. *Philosophical Transactions of the Royal Society of London A: Mathematical, Physical and Engineering Sciences* **366**, 195–204 (2008).
120. Couto, N. J. *et al.* Random strain fluctuations as dominant disorder source for high-quality on-substrate graphene devices. *Physical Review X* **4**, 041019 (2014).
121. Engels, S. *et al.* Limitations to carrier mobility and phase-coherent transport in bilayer graphene. *Physical review letters* **113**, 126801 (2014).
122. Charlier, J.-C. Defects in carbon nanotubes. *Accounts of chemical research* **35**, 1063–1069 (2002).
123. Monteverde, M. *et al.* Transport and elastic scattering times as probes of the nature of impurity scattering in single-layer and bilayer graphene. *Physical review letters* **104**, 126801 (2010).
124. Van Tuan, D. *et al.* Scaling properties of charge transport in polycrystalline graphene. *Nano letters* **13**, 1730–1735 (2013).
125. Cummings, A. W. *et al.* Charge transport in polycrystalline graphene: challenges and opportunities. *Advanced Materials* **26**, 5079–5094 (2014).
126. Woessner, A. *et al.* Near-field photocurrent nanoscopy on bare and encapsulated graphene. *Nature communications* **7**, 10783 (2016).
127. Geringer, V. *et al.* Intrinsic and extrinsic corrugation of monolayer graphene deposited on SiO2. *Physical review letters* **102**, 076102 (2009).
128. Müller, M. & Sachdev, S. Collective cyclotron motion of the relativistic plasma in graphene. *Physical Review B* **78**, 115419 (2008).
129. Foster, M. S. & Aleiner, I. L. Slow imbalance relaxation and thermoelectric transport in graphene. *Physical Review B* **79**, 085415 (2009).
130. Van Tuan, D. *et al.* Insulating behavior of an amorphous graphene membrane. *Physical Review B* **86**, 121408 (2012).
131. Dubois, S. M.-M. *et al.* Quantum transport in graphene nanoribbons: Effects of edge reconstruction and chemical reactivity. *Acs Nano* **4**, 1971–1976 (2010).
132. Peng, X., Wei, Q. & Copple, A. Strain-engineered direct-indirect band gap transition and its mechanism in two-dimensional phosphorene. *Physical Review B* **90**, 085402 (2014).
133. Han, X., Stewart, H. M., Shevlin, S. A., Catlow, C. R. A. & Guo, Z. X. Strain and orientation modulated bandgaps and effective masses of phosphorene nanoribbons. *Nano letters* **14**, 4607–4614 (2014).
134. Tran, V., Soklaski, R., Liang, Y. & Yang, L. Layer-controlled band gap and anisotropic excitons in few-layer black phosphorus. *Physical Review B* **89**, 235319 (2014).
135. Hu, T. & Hong, J. Anisotropic effective mass, optical property, and enhanced band gap in BN/phosphorene/BN heterostructures. *ACS applied materials & interfaces* **7**, 23489–23495 (2015).
136. Liao, B., Zhou, J., Qiu, B., Dresselhaus, M. S. & Chen, G. Ab initio study of electron-phonon interaction in phosphorene. *Physical Review B* **91**, 235419 (2015).
137. Liu, Y., Low, T. & Ruden, P. P. Mobility anisotropy in monolayer black phosphorus due to scattering by charged impurities. *Physical Review B* **93**, 165402 (2016).
138. Rudenko, A., Brener, S. & Katsnelson, M. Intrinsic charge carrier mobility in single-layer black phosphorus. *Physical review letters* **116**, 246401 (2016).
139. Datta, S. *Electronic transport in mesoscopic systems*. (Cambridge university press, 1997).
140. Büttiker, M. Four-terminal phase-coherent conductance. *Physical review letters* **57**, 1761 (1986).
141. Proetto, C. Thermopower oscillations of a quantum-point contact. *Physical Review B* **44**, 9096 (1991).
142. Wang, B., Zhou, J., Yang, R. & Li, B. Ballistic thermoelectric transport in structured nanowires. *New Journal of Physics* **16**, 065018 (2014).

Acknowledgements

Author Contributions

S.T. designed and performed the research, analyzed the data and wrote the paper.

Additional Information